

A MIXED FORMULATION FOR A CONTINUUM-BASED BEAM ELEMENT

Ricardo Rodrigues Martins, ricardo.r.martins@petrobras.com.br

PETROBRAS R&D Center (CENPES), Avenida Horácio Macedo, 950, Cidade Universitária, 21941-915 Rio de Janeiro, RJ, Brazil

Nestor Zouain, nestor@ufrj.br

Lavinia Borges, lavinia@ufrj.br

Department of Mechanical Engineering, Universidade Federal do Rio de Janeiro, P.O. Box 68503, 21945-970 Rio de Janeiro, RJ, Brazil

Abstract. *The continuum-based (CB) finite element approach has been demonstrated to be a good choice for the modeling of long thin structures, providing very good results. In this technique, the element formulation starts from the classical continuum formulation. Then, assumptions on the motion and on the stress state of the elements are made so that they behave like structural elements, e.g. beams and shells. Therefore, this methodology seems to be a simpler way for developing structural elements than the use of classical theories.*

In this paper the CB approach is used for the development of a multilayer three-node beam element for the solution of 2D linear elastic problems and limit analysis using direct methods. The element displacements/velocities are quadratic along the element axis and linear through the thickness. Bilinear interpolation functions are used to interpolate the stress fields on each element layer. Continuity of the stresses through the element thickness can be also enforced. Different materials can be defined on each element layer, allowing to model composite.

The use of mixed formulation allows the easy application of the element proposed herein on the solution of plasticity problems using direct methods. The examples provided include simulations of linear elastic and limit analysis problems. The results are used to verify the robustness and accuracy of the element.

Keywords: *Beams, Finite Element Method, Mixed Formulation, Limit Analysis*

1. INTRODUCTION

Structural elements such as beams, plates and shells, are very important for modeling long thin structures especially because the use of classical continuum elements for this task is computationally very expensive due to the huge number of elements required. Moreover, modeling of long thin structures with continuum elements often leads to high aspect ratios which can cause ill conditioning of the system of equations and loss of accuracy of the solution (Belytschko *et al.*, 2001).

Structural elements can be formulated by using classical theories, e.g. Euler-Bernoulli and Timoshenko beam theories, or by developing the element directly from a classical continuum element by imposing proper structural assumptions. This second technique is named continuum based (CB) approach (and is also known as degenerate continuum approach).

In this work the CB approach is used for the development of a multilayer three-node beam element for the solution of linear elastic problems (Hughes, 1987; Bathe, 1996) and limit analysis problems using direct methods (Maier *et al.*, 2003; Zouain, 2004). Other implementations of CB beam elements for different applications can be found in (Sosa and Gil, 2009).

Particularly for plasticity problems using direct methods, structural CB elements are advantageous because the yield function can be defined the same way as for continuum elements, without any approximation. However, for classical beam elements, the yield function is approximated by using stress resultants: bending moment, shear and axial forces.

The element proposed herein is different from those originally given by Belytschko *et al.* (2001) mainly because it is developed using a mixed formulation whereas Belytschko's element employs a kinematical formulation. Nevertheless, for the solution of limit analysis problems, implementing mixed elements is easier and, in general, more appropriate than producing kinematical elements because the dissipation function for the discrete version of the kinematical formulation needs to be exactly computed, which is only possible for simple interpolation schemes (Borges, 1991).

The proposed mixed CB beam element employs an interpolation scheme compatible with the Hellinger-Reissner functional. Hence, it interpolates stress and displacement/velocity fields independently. In this case, displacements/velocities are quadratic along the element axis and linear through the thickness. Stresses are interpolated by layers using bilinear interpolation functions.

The implementation using the CB approach was easy and provided very good results, as demonstrated by the examples. Furthermore, one of the next steps of this research involves the development of shell elements for limit analysis and shakedown problems. In this case the CB technique becomes specially appealing, since it avoids dealing with the complexity of the governing equations involved in classical shell theories, mainly to describe the yield function.

The paper is structured as follows: Firstly the variational principles used to obtain the discrete versions for the linear elastic and limit analysis problems are briefly presented. Secondly, some details for implementing the finite element are provided along with the discrete versions of the variational principles previously described. Thirdly, two examples are

given to demonstrate the element performance: the first involving a linear elastic analysis of a curved beam and the second for the case of a limit analysis of a beam subjected to bending plus axial force. The results are presented and discussed. Finally, some concluding remarks are made.

2. VARIATIONAL PRINCIPLES

One of the advantages of the continuum-based element formulation for modeling beams is that governing equations for the structural element are identical to those for continua. The specialization of these equations to beams, which is performed in the next section, is made imposing the assumptions of beam theory on the motion and on the state of stress.

In this section we briefly provide the variational formulations used to obtain the discrete equations for linear elasticity and limit analysis.

2.1 Two-field mixed formulation in elasticity

The Hellinger-Reissner functional (Han and Reddy, 1999; Bathe, 1996) is given by

$$\Pi^{HR}(\hat{\sigma}, \hat{u}) = -\frac{1}{2} \int_{\mathcal{B}} \hat{\sigma} \cdot \hat{\mathbb{E}}^{-1} \hat{\sigma} d\mathcal{B} + \int_{\mathcal{B}} \hat{\sigma} \cdot \mathcal{D}\hat{u} d\mathcal{B} - \int_{\mathcal{B}} \hat{u} \cdot \hat{b} d\mathcal{B} - \int_{\Gamma_{\tau}} \hat{u} \cdot \hat{\tau} d\Gamma_{\tau} \quad (1)$$

Invoking the stationarity of its first variation ($\delta\Pi^{HR}(\hat{\sigma}, \hat{u}) = 0$) one can arrive at the following variational or weak formulation, used for the development of the mixed CB beam for linear elastic problems:

Given the prescribed body forces \hat{b} acting on \mathcal{B} and the boundary tractions $\hat{\tau}$ applied on the part Γ_{τ} of the boundary Γ of \mathcal{B} , find the displacement field $\hat{u} \in \mathcal{V}$ and stress field $\hat{\sigma} \in \mathcal{W}'$ that satisfy

$$\int_{\mathcal{B}} \delta\hat{\sigma} \cdot \mathcal{D}\hat{u} d\mathcal{B} - \int_{\mathcal{B}} \delta\hat{\sigma} \cdot \hat{\mathbb{E}}^{-1} \hat{\sigma} d\mathcal{B} = 0 \quad \forall \quad \delta\hat{\sigma} \in \mathcal{W}' \quad (2)$$

$$\int_{\mathcal{B}} \hat{\sigma} \cdot \mathcal{D}\delta\hat{u} d\mathcal{B} - \int_{\mathcal{B}} \delta\hat{u} \cdot \hat{b} d\mathcal{B} - \int_{\Gamma_{\tau}} \delta\hat{u} \cdot \hat{\tau} d\Gamma_{\tau} = 0 \quad \forall \quad \delta\hat{u} \in \mathcal{V} \quad (3)$$

The space \mathcal{V} consists of all vector fields sufficiently regular and satisfying homogeneous constraints in the part $\Gamma_{\mathbf{u}}$, of the boundary Γ of \mathcal{B} . Note that since the first derivative of \hat{u} and its variation $\delta\hat{u}$ appears in Eq. (2) and Eq. (3), respectively, elements of \mathcal{V} should have integrable derivatives, that in this case implies $\hat{u}, \delta\hat{u} \in C^0$.

On the other hand, the field space \mathcal{W}' comprises less regular functions. In fact, the elements of \mathcal{W}' are symmetric tensor fields which can be piecewise continuous functions, i.e., $\hat{\sigma}, \delta\hat{\sigma} \in C^{-1}$. The dual space of \mathcal{W}' is the space of admissible strain fields \mathcal{W} .

The boundary partition, $\Gamma_{\mathbf{u}}$ and Γ_{τ} , is such that $\Gamma_{\mathbf{u}} \cup \Gamma_{\tau} = \Gamma$ and $\Gamma_{\mathbf{u}} \cap \Gamma_{\tau}$ is empty.

The fourth order tensor $\hat{\mathbb{E}}$ determines the elastic stress-strain relation, and \mathcal{D} is the tangent deformation operator which maps \mathcal{V} into \mathcal{W} . Then, $\hat{\sigma} = \hat{\mathbb{E}}\hat{\varepsilon}$ and $\hat{\varepsilon} = \mathcal{D}\hat{u}$, $\hat{\varepsilon} \in \mathcal{W}$.

2.2 Limit Analysis

Under the assumptions of proportional loading, infinitesimal strains and small displacements, the limit analysis problem consists of finding a load factor α such that the body undergoes plastic collapse. For ductile structures when subjected to the reference loads $F \in \mathcal{V}'$ uniformly amplified by α , plastic collapse happens when its load carrying capacity is exhausted. The symbol \mathcal{V}' denotes the space of load systems F which is the dual space of \mathcal{V} . In turn, a system of loads produces plastic collapse if there exists a stress field in equilibrium with these loads which is plastically admissible, and related, by constitutive equations, to a plastic strain rate field being kinematically admissible (Lubliner, 1990; Borges *et al.*, 2001).

Thus, the limit analysis problem consist of finding $\alpha \in \mathbb{R}$, a stress field $\hat{\sigma} \in \mathcal{W}'$, a plastic strain rate field $\hat{d}^p \in \mathcal{W}$ and a velocity field $\hat{v} \in \mathcal{V}$ such that

$$\hat{d}^p = \mathcal{D}\hat{v}, \quad \hat{v} \in \mathcal{V}, \quad (4)$$

$$\hat{\sigma} \in S(\alpha F), \quad (5)$$

$$\hat{\sigma} \in \partial X(\hat{d}^p). \quad (6)$$

Equation (4) imposes that plastic strain rate $\hat{\mathbf{d}}^p$ is related to a kinematically admissible velocity field $\hat{\mathbf{v}}$ by means of \mathcal{D} . The symbol $S(\alpha F)$ in Eq. (5) denotes the set of all stress fields in equilibrium with the given system of forces αF , i.e., satisfying the principle of virtual power:

$$\int_{\mathcal{B}} \hat{\boldsymbol{\sigma}} \cdot \mathcal{D}\hat{\mathbf{v}}d\mathcal{B} = \alpha \left(\int_{\mathcal{B}} \delta\hat{\mathbf{v}} \cdot \hat{\mathbf{b}}d\mathcal{B} + \int_{\Gamma_{\tau}} \delta\hat{\mathbf{v}} \cdot \hat{\boldsymbol{\tau}}d\Gamma_{\tau} \right) \quad \forall \quad \delta\hat{\mathbf{v}} \in \mathcal{V} \quad (7)$$

Equation (6) gives the constitutive relation describing an elastic ideally plastic material. The symbol $\partial X(\hat{\mathbf{d}}^p)$ denotes the subdifferential of the plastic dissipation function X , which is the set of all stress fields, such that

$$X(\hat{\mathbf{d}}^{p*}) - X(\hat{\mathbf{d}}^p) \geq \int_{\mathcal{B}} \hat{\boldsymbol{\sigma}} \cdot (\hat{\mathbf{d}}^{p*} - \hat{\mathbf{d}}^p)d\mathcal{B} \quad \forall \hat{\mathbf{d}}^{p*} \in W. \quad (8)$$

The dissipation function is related to the set P of plastically admissible stress fields by

$$X(\hat{\mathbf{d}}^p) = \sup_{\hat{\boldsymbol{\sigma}}^* \in P} \int_{\mathcal{B}} \hat{\boldsymbol{\sigma}}^* \cdot \mathcal{D}\hat{\mathbf{v}}d\mathcal{B} \quad (9)$$

Frequently, the set P is defined as

$$P = \{ \hat{\boldsymbol{\sigma}} \in \mathcal{W}' \mid f(\hat{\boldsymbol{\sigma}}) \leq 0 \quad \text{in} \quad \mathcal{B} \} \quad (10)$$

where the above inequality is understood as imposing that each component f_k , which is a regular convex function of $\hat{\boldsymbol{\sigma}}$, is non-positive. Then, at any point of \mathcal{B} , Eq. (7) is equivalent to the normality rule $\hat{\mathbf{d}}^p = \nabla f(\hat{\boldsymbol{\sigma}})\hat{\boldsymbol{\lambda}}$, where $\nabla f(\hat{\boldsymbol{\sigma}})$ denotes the gradient of f , and $\hat{\boldsymbol{\lambda}}$ is the \hat{m} -vector of field plastic multipliers. At any point of \mathcal{B} , the components of $\hat{\boldsymbol{\lambda}}$ are related to each plastic mode in f by the complementary condition $\hat{\lambda} \geq 0$, $f \leq 0$ and $\hat{\lambda}f = 0$ (these inequalities hold componentwise). The classical extremum principles of limit analysis, i.e., the kinematical, statical and mixed formulations, can be derived from optimality conditions, Eq. (4)-(6) (Christiansen, 1996; Borges *et al.*, 1996). The discretized versions of these formulations lead to a single type of finite dimensional problem, which can be given in four strictly equivalent forms, namely the statical, mixed and kinematical discrete formulations, and the set of discrete optimality conditions.

3. FINITE ELEMENT DISCRETIZATION

3.1 Basic nomenclature for mixed CB beam elements

Figure 1 shows a 2-D mixed CB element and its respective parent element. Local coordinates of the parent element are represented by ξ and η whereas global coordinates are given by x and y . As can be seen, mixed CB elements have three different kinds of nodes: master, slave and stress nodes. Master nodes are represented by black dots. Its degrees of freedom (d.o.f.), two displacements u_x^I and u_y^I and one rotation ω^I , $I = 1, \dots, 3$, describe the motion of the beam. The line connecting master nodes is called reference line. Its position is arbitrary, and in this case it is chosen to coincide with the mid line of the beam ($\eta = 0$).

The element has 6 “slave” nodes which define the underlying continuum element of the CB beam element. These nodes are called slave because their displacements/velocities are determined by those from the respective master nodes. Adopting the same nomenclature of Belytschko *et al.* (2001), lines of constant ξ are called fibers. Each master node is connected to the pair of slave nodes lying on the same fiber. Lines of constant η are named laminae.

The unit vectors \mathbf{p} aligned with the fibers are called directors or pseudonormals. They are used to describe the element kinematics like normals in the classical beam theory. However, directors are not necessarily normal. Directors also determine the coordinates of slave nodes.

Stress nodes, represented by squares in Fig. 1, are used to interpolate the stress field in each element layer. The number of layers (nc) depends on the kind of problem. To model beams made of homogeneous elastic material, only one layer is needed. On the other hand, for limit analysis the accuracy of the response is highly dependent on the number of layers. Particularly for the examples in this paper 8 layers proved to be adequate.

3.2 Assumptions

For the development of the CB Beam element, the following hypotheses are assumed:

1. The fibers remain straight;
2. The transverse normal stress is negligible;
3. The fibers are inextensible.

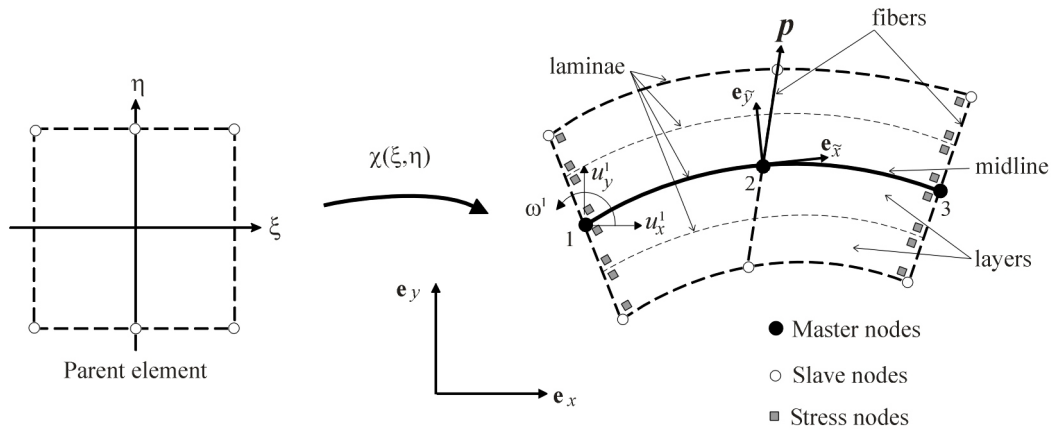


Figure 1. Three-node mixed continuum based (CB) beam element

Although there is a contradiction between the hypotheses 2 and 3, this also happens in classical beam theory. An approach to solve this inconsistency is to calculate the normal strain not from the motion but via constitutive equations (Belytschko *et al.*, 2001), allowing to consider changes in element thickness. See also (Lembo and Podio-Guidugli, 2001) for a consistent bending theory.

3.3 Interpolation of displacement/velocity and stress fields

The discrete form of the variational principles described in the previous section is obtained by approximating displacement/velocity and stress fields of the underlying continuum element using standard Lagrange finite element shape functions.

The plane stress assumption (hypothesis 2) have to be imposed to convert the underlying element from a standard continuum element to a CB element. This is performed firstly defining the components of the interpolated fields using a corotational or lamina coordinate system. Corotational components are indicated using a superposed $\tilde{\cdot}$. Then, the condition that $\tilde{\sigma}_y = 0$ for each point of the underlying continuum element is enforced.

The base vectors of the corotational system, depicted in Fig. 1, are constructed so that, for each point of the underlying continuum element, $\mathbf{e}_{\tilde{x}}$ is tangent to the lamina and $\mathbf{e}_{\tilde{y}} \perp \mathbf{e}_{\tilde{x}}$.

Defining the parent coordinates of the CB element as ξ and η , the corotational basis $\{\mathbf{e}_{\tilde{x}}, \mathbf{e}_{\tilde{y}}\}$ is related to the global basis $\{\mathbf{e}_x, \mathbf{e}_y\}$ as follows (Sosa and Gil, 2009):

$$\begin{bmatrix} \mathbf{e}_{\tilde{x}} \\ \mathbf{e}_{\tilde{y}} \end{bmatrix} = \begin{bmatrix} \frac{x_{,\xi}}{\sqrt{x_{,\xi}^2 + y_{,\xi}^2}} & \frac{y_{,\xi}}{\sqrt{x_{,\xi}^2 + y_{,\xi}^2}} \\ \frac{-y_{,\xi}}{\sqrt{x_{,\xi}^2 + y_{,\xi}^2}} & \frac{x_{,\xi}}{\sqrt{x_{,\xi}^2 + y_{,\xi}^2}} \end{bmatrix} \begin{bmatrix} \mathbf{e}_x \\ \mathbf{e}_y \end{bmatrix} \quad (11)$$

where $x_{,\xi}$ and $y_{,\xi}$ are the derivatives of coordinates x and y of the considered point of the CB element with respect to the parent coordinate ξ .

3.3.1 Interpolation of displacement/velocity fields

Interpolated displacement/velocities fields \mathbf{u} and \mathbf{v} were assumed to be continuous through elements. The element displacements/velocities are quadratic in ξ direction and linear in η direction. The shape functions for these fields, written in matrix form, are

$$\mathbf{N}_v = [g_1 \mathbf{1}_2 \quad g_2 \mathbf{1}_2 \quad g_3 \mathbf{1}_2 \quad g_4 \mathbf{1}_2 \quad g_5 \mathbf{1}_2 \quad g_6 \mathbf{1}_2] \quad (12)$$

where $\mathbf{1}_2$ is the 2×2 identity matrix and g_i are the following functions (Hughes, 1987):

$$\begin{aligned} g_1 &= \frac{1}{4}\xi(\xi - 1)(1 - \eta) \\ g_2 &= \frac{1}{4}\xi(\xi - 1)(1 + \eta) \\ g_3 &= \frac{1}{2}(1 - \xi)(1 + \xi)(1 - \eta) \\ g_4 &= \frac{1}{2}(1 - \xi)(1 + \xi)(1 + \eta) \\ g_5 &= \frac{1}{4}\xi(\xi + 1)(1 - \eta) \\ g_6 &= \frac{1}{4}\xi(\xi + 1)(1 + \eta) \end{aligned} \quad (13)$$

Displacement/velocities vectors at slave nodes of element e are:

$$\begin{aligned} \mathbf{u}_s^e &= [u_x^{s1} \ u_y^{s1} \ \dots \ u_x^{s6} \ u_y^{s6}]^T \\ \mathbf{v}_s^e &= [v_x^{s1} \ v_y^{s1} \ \dots \ v_x^{s6} \ v_y^{s6}]^T \end{aligned} \quad (14)$$

The vectors that store the d.o.f. of master nodes are:

$$\begin{aligned} \mathbf{u}^e &= [u_x^1 \ u_y^1 \ \omega^1 \ \dots \ u_x^3 \ u_y^3 \ \omega^3]^T \\ \mathbf{v}^e &= [v_x^1 \ v_y^1 \ \dot{\omega}^1 \ \dots \ v_x^3 \ v_y^3 \ \dot{\omega}^3]^T \end{aligned} \quad (15)$$

It is emphasized that the interpolated fields are represented using components in the corotational coordinate system, whereas the d.o.f. of master and slave nodes are chosen in the global coordinate system. The matrix that transforms the displacement/velocity vectors of slave nodes from the corotational coordinate system to the global coordinate system is given by:

$$\mathbf{R} = \begin{bmatrix} \mathbf{R} & \mathbf{0} & \mathbf{0} & \mathbf{0} & \mathbf{0} & \mathbf{0} \\ \mathbf{0} & \mathbf{R} & \mathbf{0} & \mathbf{0} & \mathbf{0} & \mathbf{0} \\ \mathbf{0} & \mathbf{0} & \mathbf{R} & \mathbf{0} & \mathbf{0} & \mathbf{0} \\ \mathbf{0} & \mathbf{0} & \mathbf{0} & \mathbf{R} & \mathbf{0} & \mathbf{0} \\ \mathbf{0} & \mathbf{0} & \mathbf{0} & \mathbf{0} & \mathbf{R} & \mathbf{0} \\ \mathbf{0} & \mathbf{0} & \mathbf{0} & \mathbf{0} & \mathbf{0} & \mathbf{R} \end{bmatrix} \quad \text{where,} \quad \mathbf{R} = \begin{bmatrix} \mathbf{e}_x \cdot \mathbf{e}_{\bar{x}} & \mathbf{e}_y \cdot \mathbf{e}_{\bar{x}} \\ \mathbf{e}_x \cdot \mathbf{e}_{\bar{y}} & \mathbf{e}_y \cdot \mathbf{e}_{\bar{y}} \end{bmatrix} \quad (16)$$

The matrix that relates velocity/displacement components of slave nodes to degrees of freedom of master nodes, both in the global coordinate system, is:

$$\mathbf{T} = \begin{bmatrix} \mathbf{T}_1 & \mathbf{0} & \mathbf{0} \\ \mathbf{0} & \mathbf{T}_2 & \mathbf{0} \\ \mathbf{0} & \mathbf{0} & \mathbf{T}_3 \end{bmatrix} \quad \text{where,} \quad \mathbf{T}_I = \begin{bmatrix} 1 & 0 & y_I - y_{I-} \\ 0 & 1 & x_I - x_{I-} \\ 1 & 0 & y_I - y_{I+} \\ 0 & 1 & x_I - x_{I+} \end{bmatrix} \quad (17)$$

Subscripts I^- and I^+ are used to identify slave nodes located below and above the master node I . Hence, symbols x_I and y_I denote global coordinates of the master node I and symbols $x_{I-}, y_{I-}, x_{I+}, y_{I+}$ represent the global coordinates of slave nodes I^- and I^+ . The matrix \mathbf{T}_I connects the degrees of freedom of the master node I with the degrees of freedom of its pair of slave nodes.

Using the above definitions, we obtain the following equations for displacement and velocity fields of the element e :

$$\begin{aligned} \tilde{\mathbf{u}} &= \mathbf{N}_v \tilde{\mathbf{u}}_s^e = \mathbf{N}_v \mathbf{R} \mathbf{u}_s^e = \mathbf{N}_v \mathbf{R} \mathbf{T} \mathbf{u}^e \\ \tilde{\mathbf{v}} &= \mathbf{N}_v \tilde{\mathbf{v}}_s^e = \mathbf{N}_v \mathbf{R} \mathbf{v}_s^e = \mathbf{N}_v \mathbf{R} \mathbf{T} \mathbf{v}^e \end{aligned} \quad (18)$$

Analogously, the equations for the fields $\delta \mathbf{u}$ and $\delta \mathbf{v}$ are

$$\begin{aligned} \delta \tilde{\mathbf{u}} &= \mathbf{N}_v \delta \tilde{\mathbf{u}}_s^e = \mathbf{N}_v \mathbf{R} \delta \mathbf{u}_s^e = \mathbf{N}_v \mathbf{R} \mathbf{T} \delta \mathbf{u}^e \\ \delta \tilde{\mathbf{v}} &= \mathbf{N}_v \delta \tilde{\mathbf{v}}_s^e = \mathbf{N}_v \mathbf{R} \delta \mathbf{v}_s^e = \mathbf{N}_v \mathbf{R} \mathbf{T} \delta \mathbf{v}^e \end{aligned} \quad (19)$$

3.3.2 Interpolation of stress field

The interpolated stress field is assumed to be discontinuous through elements. Stress interpolation is performed in each element first dividing the element in nc layers (see Fig.1).

Then, stress nodes are placed in each layer corner. If continuity of stress field between adjacent layers is enforced, nodes at common boundaries are shared. Otherwise, each layer has its own set of four nodes, as depicted in Fig. 1.

Next, stress fields $\tilde{\boldsymbol{\sigma}}$ and $\delta \tilde{\boldsymbol{\sigma}}$ in each element layer c of the e -th element are approximated by

$$\begin{aligned} \tilde{\boldsymbol{\sigma}} &= \mathbf{N}_{\boldsymbol{\sigma}} (\tilde{\boldsymbol{\sigma}}^c)^e \\ \delta \tilde{\boldsymbol{\sigma}} &= \mathbf{N}_{\boldsymbol{\sigma}} (\delta \tilde{\boldsymbol{\sigma}}^c)^e \end{aligned} \quad (20)$$

using the following shape functions:

$$\mathbf{N}_{\boldsymbol{\sigma}} = [t_1 \mathbf{1}_2 \quad t_2 \mathbf{1}_2 \quad t_3 \mathbf{1}_2 \quad t_4 \mathbf{1}_2] \quad (21)$$

where, $t_j = \frac{1}{4}(1 + \xi_j \xi)(1 + \eta_j \eta)$ are standard Lagrange bilinear functions; the coefficients ξ_j and η_j , $j = 1, \dots, 4$, are the coordinates of the vertices of the layer c in the parent element; $(\tilde{\boldsymbol{\sigma}}^c)^e$ and $(\delta \tilde{\boldsymbol{\sigma}}^c)^e$, given as follows, are the vectors that store stress coefficients of each layer.

$$\begin{aligned} (\tilde{\boldsymbol{\sigma}}^c)^e &= [\tilde{\sigma}_x^{1/c} \ \sqrt{2} \tilde{\sigma}_{xy}^{1/c} \ \dots \ \tilde{\sigma}_x^{4/c} \ \sqrt{2} \tilde{\sigma}_{xy}^{4/c}]^T \\ (\delta \tilde{\boldsymbol{\sigma}}^c)^e &= [\delta \tilde{\sigma}_x^{1/c} \ \sqrt{2} \delta \tilde{\sigma}_{xy}^{1/c} \ \dots \ \delta \tilde{\sigma}_x^{4/c} \ \sqrt{2} \delta \tilde{\sigma}_{xy}^{4/c}]^T \end{aligned} \quad (22)$$

Finally, the vectors of stress coefficients of the element e , $\tilde{\sigma}^e$ and $\delta\tilde{\sigma}^e$, are defined. These are obtained by assembling the vectors of each layer c using standard finite element procedures and taking into account if there are shared degrees of freedom between adjacent layers.

It is noteworthy to mention that for limit analysis, due to the convexity of the set P of plastically admissible stresses, the piecewise linear functions chosen to interpolate the stress fields (see Eq. 20) enforces these approximated fields to be plastically admissible. This is advantageous because plastic admissibility of stresses needs to be only verified at the stress nodes to guarantee that the same happens in all element domain. Moreover, the inter-element discontinuity of interpolated stresses leads to a global vector of stress parameters which is made up of disjoint sets of vectors corresponding to each element. Then, the set of plastic admissibility constraints of each element e is only dependent on the separate set of stress components of that element. This uncoupling also has important consequences for the computational feasibility of the discrete limit analysis algorithm (Borges *et al.*, 1996).

3.4 Matrix form of the linear elastic problem

The classical matrix form for the linear elastic problem is obtained firstly dividing the domain \mathcal{B} in Eq. (2) and Eq. (3) in ne elements, each element with nc layers. Then, displacement and stress fields are replaced by their respective approximate fields, see Eq. (18), Eq. (19) and Eq. (22). Next, after some algebraic manipulation, one can obtain $\mathbf{K}\mathbf{u} = \mathbf{F}$, where: \mathbf{K} is the global stiffness matrix; \mathbf{F} is the load vector and \mathbf{u} is the vector of unknown displacements at master nodes.

The global stiffness matrix is given by

$$\mathbf{K} = \sum_{e=1}^{ne} \mathbf{K}^e \quad \text{where,} \quad \mathbf{K}^e = (\tilde{\mathbf{B}}^e)^T \tilde{\mathbb{E}}^e \tilde{\mathbf{B}}^e \quad (e\text{-th element stiffness matrix}) \quad (23)$$

The load vector \mathbf{F} is computed as

$$\mathbf{F} = \int_{\mathcal{B}} \mathbf{N}_v^T \hat{\mathbf{b}} d\mathcal{B} + \int_{\Gamma_\tau} \mathbf{N}_v^T \hat{\tau} d\Gamma_\tau \quad (24)$$

Matrices $\tilde{\mathbf{B}}^e$ and $\tilde{\mathbb{E}}^e$ are respectively the discrete deformation operator and the discrete elastic relation of element e . The way that these matrices are obtained is explained in what follows, only for the case that the interpolated stress field is discontinuous through layers.

3.4.1 Discrete deformation operator

In order to compute the discrete deformation operator $\tilde{\mathbf{B}}^e$ we first compute $\tilde{\mathbf{B}}^c$, the contributions of each element layer c as follows

$$\tilde{\mathbf{B}}^c = \int_{\mathcal{B}^c} \mathbf{N}_\sigma^T \tilde{\mathcal{D}} \mathbf{N}_v \mathbf{R} d\mathcal{B}^c = \int_{\mathcal{B}^c} [\mathbf{A}^1 \quad \dots \quad \mathbf{A}^6] \mathbf{R} d\mathcal{B}^c \quad (25)$$

The deformation operator $\tilde{\mathcal{D}}$ is defined to be compatible with the plane stress assumption. Hence

$$\tilde{\mathcal{D}} \mathbf{N}_v = \left[\tilde{\mathbf{B}}^1 \quad \dots \quad \tilde{\mathbf{B}}^6 \right] \quad \text{where} \quad \tilde{\mathbf{B}}^k = \begin{bmatrix} g_{k,\bar{x}} & 0 \\ \frac{1}{\sqrt{2}} g_{k,\bar{y}} & \frac{1}{\sqrt{2}} g_{k,\bar{x}} \end{bmatrix} \quad (26)$$

$$\text{and} \quad \mathbf{A}^k = \begin{bmatrix} t_1 g_{k,\bar{x}} & 0 \\ \frac{1}{\sqrt{2}} t_1 g_{k,\bar{y}} & \frac{1}{\sqrt{2}} t_1 g_{k,\bar{x}} \\ t_2 g_{k,\bar{x}} & 0 \\ \frac{1}{\sqrt{2}} t_2 g_{k,\bar{y}} & \frac{1}{\sqrt{2}} t_2 g_{k,\bar{x}} \\ t_3 g_{k,\bar{x}} & 0 \\ \frac{1}{\sqrt{2}} t_3 g_{k,\bar{y}} & \frac{1}{\sqrt{2}} t_3 g_{k,\bar{x}} \\ t_4 g_{k,\bar{x}} & 0 \\ \frac{1}{\sqrt{2}} t_4 g_{k,\bar{y}} & \frac{1}{\sqrt{2}} t_4 g_{k,\bar{x}} \end{bmatrix} \quad (27)$$

Finally, the discrete deformation operator for the element e is assembled as follows

$$\tilde{\mathbf{B}}^e = \left\{ \sum_{c=1}^{nc} \int_{\mathcal{B}^c} \mathbf{N}_\sigma^T \tilde{\mathcal{D}} \mathbf{N}_v \mathbf{R} d\mathcal{B}^c \right\} \mathbf{T} = \sum_{c=1}^{nc} \tilde{\mathbf{B}}^c \mathbf{T} = \begin{bmatrix} \tilde{\mathbf{B}}^1 \\ \vdots \\ \tilde{\mathbf{B}}^{nc} \end{bmatrix} \mathbf{T} \quad (28)$$

3.4.2 Discrete elastic relation

The discrete elastic relation $\tilde{\mathbb{E}}^e$ is also calculated computing and assembling the contributions of each element layer c , in this case $\hat{\mathbb{E}}^c$, such that

$$(\tilde{\mathbb{E}}^e)^{-1} = \sum_{c=1}^{nc} (\hat{\mathbb{E}}^c)^{-1} \quad \text{where} \quad (\hat{\mathbb{E}}^c)^{-1} = \int_{\mathcal{B}^c} \mathbf{N}_\sigma^T \hat{\mathbb{E}}^{-1} \mathbf{N}_\sigma d\mathcal{B}^c \quad (29)$$

The stress-strain relation (elastic relation) $\hat{\mathbb{E}}$ in the equation above considering the plane stress constraint ($\tilde{\sigma}_y = 0$) is

$$\hat{\mathbb{E}} = E \begin{bmatrix} 1 & 0 \\ 0 & \frac{1}{1+\nu} \end{bmatrix} \quad (30)$$

For now on the simplified notation $\mathbf{n} = \hat{\mathbb{E}}$ and $\mathbf{m} = \hat{\mathbb{E}}^{-1}$ is used. Thus, the following equation can be written (see Eq. (21) and Eq. (29))

$$(\tilde{\mathbb{E}}^c)^{-1} = \int_{\mathcal{B}^c} \mathbf{N}_\sigma^T \hat{\mathbb{E}}^{-1} \mathbf{N}_\sigma d\mathcal{B}^c = \int_{\mathcal{B}^c} \begin{bmatrix} t_1^2 \mathbf{m} & t_1 t_2 \mathbf{m} & t_1 t_3 \mathbf{m} & t_1 t_4 \mathbf{m} \\ t_1 t_2 \mathbf{m} & t_2^2 \mathbf{m} & t_2 t_3 \mathbf{m} & t_2 t_4 \mathbf{m} \\ t_1 t_3 \mathbf{m} & t_2 t_3 \mathbf{m} & t_3^2 \mathbf{m} & t_3 t_4 \mathbf{m} \\ t_1 t_4 \mathbf{m} & t_2 t_4 \mathbf{m} & t_3 t_4 \mathbf{m} & t_4^2 \mathbf{m} \end{bmatrix} d\mathcal{B}^c \quad (31)$$

Next, if the stress field is discontinuous through layers, the integral in Eq. (31) for each element layer can be calculated first computing and inverting for each layer c the auxiliary matrix \mathbf{a}^c such that

$$(\mathbf{a}^c)^{-1} = \int_{\mathcal{B}} \begin{bmatrix} t_1^2 & t_1 t_2 & t_1 t_3 & t_1 t_4 \\ t_1 t_2 & t_2^2 & t_2 t_3 & t_2 t_4 \\ t_1 t_3 & t_2 t_3 & t_3^2 & t_3 t_4 \\ t_1 t_4 & t_2 t_4 & t_3 t_4 & t_4^2 \end{bmatrix} d\mathcal{B} \quad (32)$$

Then, the matrices $\tilde{\mathbb{E}}^c$ are calculated and finally assembled in $\tilde{\mathbb{E}}^e$ as shown in the equations below

$$\tilde{\mathbb{E}}^c = \begin{bmatrix} a_{11}^c \mathbf{n} & a_{12}^c \mathbf{n} & a_{13}^c \mathbf{n} & a_{14}^c \mathbf{n} \\ a_{21}^c \mathbf{n} & a_{22}^c \mathbf{n} & a_{23}^c \mathbf{n} & a_{24}^c \mathbf{n} \\ a_{31}^c \mathbf{n} & a_{32}^c \mathbf{n} & a_{33}^c \mathbf{n} & a_{34}^c \mathbf{n} \\ a_{41}^c \mathbf{n} & a_{42}^c \mathbf{n} & a_{43}^c \mathbf{n} & a_{44}^c \mathbf{n} \end{bmatrix} \quad \text{and} \quad \tilde{\mathbb{E}}^e = \begin{bmatrix} \tilde{\mathbb{E}}^1 & \mathbf{0} & \dots & \mathbf{0} \\ \mathbf{0} & \tilde{\mathbb{E}}^2 & \dots & \mathbf{0} \\ \vdots & \vdots & \ddots & \vdots \\ \mathbf{0} & \mathbf{0} & \dots & \tilde{\mathbb{E}}^{nc} \end{bmatrix} \quad (33)$$

3.5 Discrete form of the limit analysis problem

The discrete limit analysis problem consists of finding a load factor $\alpha \in \mathbb{R}$, a stress vector $\boldsymbol{\sigma} \in \mathbb{R}^q$, a velocity vector $\mathbf{v} \in \mathbb{R}^n$ and a plastic multipliers vector $\dot{\boldsymbol{\lambda}} \in \mathbb{R}^m$ such that the system represented by a deformation matrix $\mathcal{B} : \mathbb{R}^n \rightarrow \mathbb{R}^q$ and a convex function $f(\boldsymbol{\sigma}) \in \mathbb{R}^m$ undergoes plastic collapse for some load being proportional to a given force vector $\mathbf{F} \in \mathbb{R}^n$. The matrix \mathcal{B} is obtained by assembling the elementary contributions $\tilde{\mathcal{B}}^e$ (see Eq. (28)). It is assumed that all rigid motions are ruled out by the kinematical constraints so that the kernel of \mathcal{B} contains only the null velocity vector.

The discretized version of the limit analysis formulation leads to a finite dimensional problem that can be seen as the discrete version of Eq. (4)-(6), that is

$$\mathcal{B}\mathbf{v} - \nabla f(\boldsymbol{\sigma})\dot{\boldsymbol{\lambda}} = 0, \quad (34)$$

$$\mathcal{B}^T \boldsymbol{\sigma} - \alpha \mathbf{F} = 0, \quad (35)$$

$$\mathbf{F} \cdot \mathbf{v} = 1, \quad (36)$$

$$f_j(\boldsymbol{\sigma})\dot{\lambda}_j = 0, \quad f_j(\boldsymbol{\sigma}) \leq 0, \quad \dot{\lambda}_j \geq 0, \quad j = 1, \dots, m. \quad (37)$$

In particular, for the mixed continuum based beam element, the yield function f is assumed to be

$$f = \tilde{\sigma}_x^2 + 3c_s\tilde{\sigma}_{xy}^2 - \sigma_Y^2 \quad (38)$$

which is the von Mises equation considering only the non-zero stress components of the element. The parameter c_s is a coefficient to consider contribution of the shear stresses to yielding. This coefficient can be set equal to 0 or 1. Therefore, if $c_s = 0$ the classical beam theory is simulated. Otherwise, $c_s = 1$ and shear stresses are considered.

The discrete limit analysis problem is solved using a nonlinear optimization Newton-like algorithm where the plastic behavior is described by means of a multimodal nonlinear yield function. This algorithm is described in (Borges *et al.*, 1996) and, for the sake of conciseness, is not discussed in this paper.

4. NUMERICAL EXAMPLES

The performance of the proposed element for linear elastic solution of thick to thin beams is presented in the first example. In the last example the element is used to achieve the load that cause instantaneous plastic collapse in a beam subjected to an axial force N and a bending moment M . For both examples the hypothesis of small displacements is assumed.

4.1 Linear elastic solution of a curved beam

The first problem, depicted in Fig. 2, consists of a semi-circular arch subjected to a vertical load $2P$. The beam has a rectangular cross-section with width b , height h , area $A_b = bh$ and moment of inertia $I = bh^3/12$. Displacements and rotation at points A and B (see Fig. 2) can be calculated by using Castigliano's energy theorem as follows:

$$u_y^{an}(A) = - \left(\frac{3\pi - 8}{4} \right) \frac{PR^3}{EI} - \frac{\pi PR}{4EA_b} - \frac{\pi PR}{4GA_bS_{cc}} \quad (39)$$

$$u_x^{an}(B) = \frac{PR^3}{2EI} - \frac{PR}{2EA_b} + \frac{PR}{2GA_bS_{cc}} \quad (40)$$

$$\omega^{an}(B) = \frac{PR^2}{EI} \left(\frac{\pi}{2} - 1 \right) \quad (41)$$

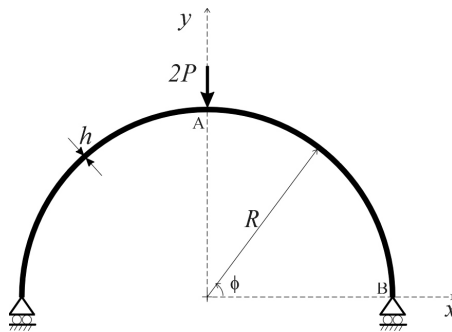


Figure 2. Semi-circular arch subjected to a load $2P$

The applied load was $P = 1.0$. The material and geometric properties are set to the following values: Young Modulus $E = 1.0 \times 10^9$, Poisson's ratio $\nu = 0.3$, shear modulus $G = E/[2(1 + \nu)]$, shear correction coefficient for a rectangular section $S_{cc} = 0.85$, $R = 10$ and $b = 1$. Four values of slenderness ratios R/h are tested: 10, 100, 700 and 1000. Due to symmetry, only a half of the structure need to be modeled with proper boundary conditions. A mesh refinement study is conducted applying four finite element meshes with increasing degrees of discretization: 1, 2, 5 and 10 elements. The elements have only one layer for stress interpolation. The third term on the RHS of Eq. (39) and Eq. (40) are the part of the displacement due to shear. These terms are usually negligible for thin beams.

Figure 3 summarize the results for the three slenderness ratios and for the four meshes. The graph on the left presents the dimensionless displacement u_y/u_y^{an} at the center of the arch (point A in Fig. 2). The graphs on the center and on the right exhibit respectively the dimensionless displacement u_x/u_x^{an} and rotation ω/ω^{an} at the support (point B in Fig. 2). It can be seen for this test that the accuracy increased with discretization. The error in the displacements remains almost stable when slenderness ratio increases and no locking is observed. Meshes with more than two elements presented errors less than 0.8%.

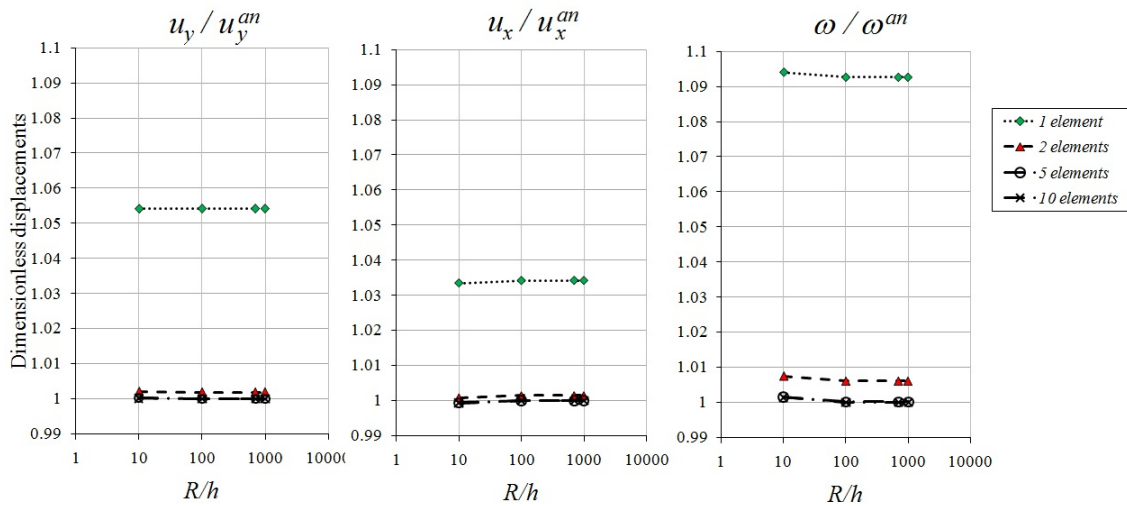


Figure 3. Element performance under various slenderness ratios

A comparison between the analytical deformed shape of the arch and the finite element results is illustratively given in Fig. 4. The results shown are for the arch with $R/h = 700$. Three distinct FE meshes with increasing degree of discretization are considered. The analytical expressions for tangential $u_t^{an}(\phi)$ and normal $u_n^{an}(\phi)$ displacements of the arch centerline were obtained neglecting contributions due to shear, and are provided in Eq. (42) and Eq. (43). It can be seen that the analytical and numerical results are in very good agreement.

$$u_t^{an}(\phi) = \frac{1}{2}R[2a \cdot \sin\phi + (2 - \pi)a \cdot \cos\phi - (a + b)\phi\cos\phi - 2a\phi - (2 - \pi)a] \quad (42)$$

$$u_n^{an}(\phi) = \frac{1}{2}R[(a + b)\cos\phi - (2 - \pi)a \cdot \sin\phi + (a + b)\phi\sin\phi - 2a] \quad (43)$$

$$\text{where, } a = \frac{R^2P}{EI} \quad \text{and} \quad b = \frac{P}{EA_b} \quad (44)$$

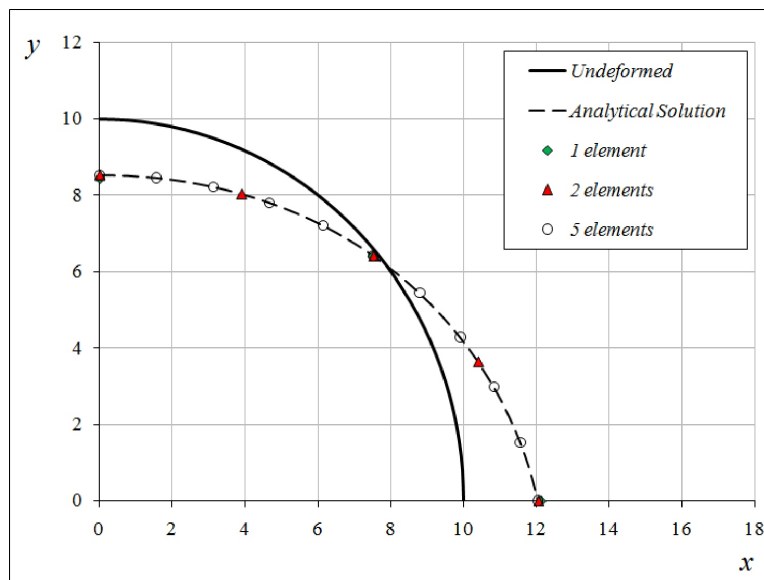


Figure 4. Deformed shape: analytical solution versus FE results

4.2 Limit analysis in tension plus bending

As an example of limit analysis consider a beam with rectangular cross section (h is the height and b is the width) under uniform external axial load N and external bending moment M , as sketched in Fig. 5.

The axial stress σ_x is a scalar function of the transversal coordinate z and the equilibrium equations are:

$$N = b \int_{-h/2}^{h/2} \sigma_x dz, \quad M = -b \int_{-h/2}^{h/2} \sigma_x z dz \quad (45)$$

The material of the beam is perfectly plastic with yield stress σ_Y . Plastic admissibility is determined by:

$$P: \quad -\sigma_Y \leq \sigma_x(z) \leq \sigma_Y \quad (46)$$

The collapse limits for pure traction and bending are, respectively, $N_Y = bh\sigma_Y$ and $M_Y = bh^2\sigma_Y/4$.

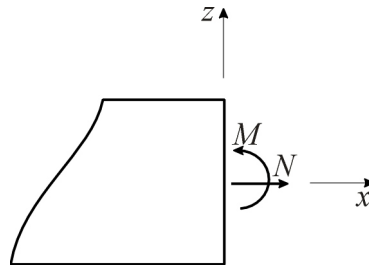


Figure 5. Beam under axial traction and bending moment

Considering that the system of loads is defined by the following non-dimensional load parameters $n = N/N_Y$ and $m = M/M_Y$ and recalling that the loading (n_c, m_c) producing instantaneous plastic collapse satisfies $n_c^2 + m_c = 1$, hence, the collapse factor α for the load (n, m) is determined analytically by solving

$$(\alpha n)^2 + \alpha m = 1 \quad (47)$$

Figure 6 depicts a comparison between the analytical solution given by Eq. (47) and the results obtained with the element proposed in this work. The beam is modeled with just one element. With the aim of assessing the effect of a better representation of the stress distribution through the thickness in the accuracy of results, different number of layers are considered: 2, 4, 8 and 16. The graph on the left presents the results obtained assuming that the stress field is discontinuous between adjacent layers whereas the graph on the right depicts the results obtained when continuity of stresses is enforced. It can be seen for the both graphs that the higher the number of layers, the closer the numerical results are to the analytical solution, as expected. For elements with 8 or more layers numerical and analytical results are quite close.

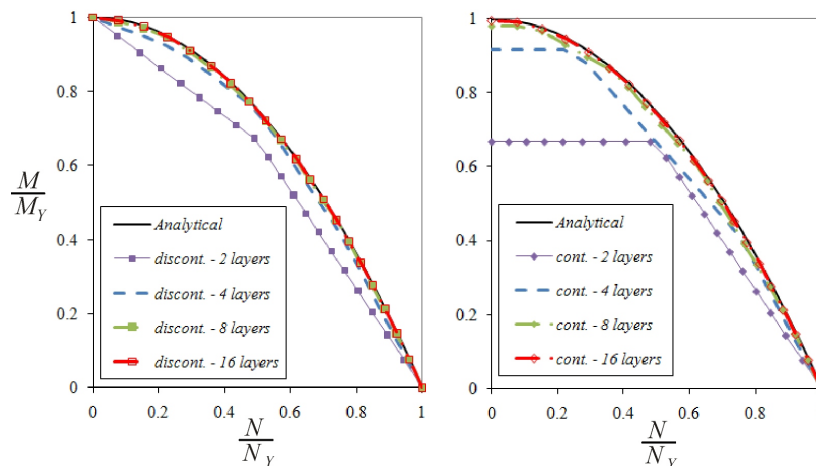


Figure 6. Bree diagram for a beam section under axial traction and bending moment: analytical solution *versus* FE results

It is also shown that, for the same number of layers, results for the element with no continuity of stress fields between layers are more accurate. The maximum differences between numerical and analytical results for the elements with 8 layers are less than 1% for the element with discontinuous stress fields and less than 3% for the element with continuity of stress fields (see Tab. 1). This better performance of elements with no continuity of stress is also predictable since axial stress distribution through the thickness is not continuous in the collapse of a beam subjected to bending plus traction.

Nevertheless, elements with no continuity of stress fields between adjacent layers are computationally much more expensive since they have almost twice stress nodes comparing to element with the same number of layers and continuity

of stress fields. This implies in more points where plastic admissibility is verified by the optimization algorithm for limit analysis increasing the computational time. Moreover, for this example, the accuracy of results of elements with similar number of stress nodes are comparable as shown in Tab. 1.

Table 1. Maximum differences between analytical and FE results

| Number of Layers | Elem. with discontinuous stress field | | Elem. with continuous stress field | |
|------------------|---------------------------------------|----------------|------------------------------------|----------------|
| | Number of stress nodes | Max. error [%] | Number of stress nodes | Max. error [%] |
| 2 | 8 | 11.1 | 6 | 33.3 |
| 4 | 16 | 2.8 | 10 | 8.4 |
| 8 | 32 | 0.7 | 18 | 2.1 |
| 16 | 64 | 0.3 | 34 | 0.5 |

5. CONCLUSION

A multilayer mixed continuum based beam element is presented for the solution of linear elastic and limit analysis problems. Details of the element implementation are given to show how to impose the structural constraint for obtaining the element from the classical continuum formulation.

The CB approach is adopted specially because for limit analysis it present advantages comparing to classical beam theory. For instance, the yield function of the CB beam element can be defined the same way as for a continuum element, without any approximation. Moreover, for the further development of shell elements this CB technique will avoid dealing with the complexity of the governing equations involved in classical shell theories.

The element proposed herein is still in development and is going to be tested for the solution of shakedown problems. However, despite the limited number of tests, for the examples given it demonstrates an excellent performance.

6. ACKNOWLEDGEMENTS

The authors would like to thank PETROBRAS for the permission to publish this paper.

7. REFERENCES

- Bathe, K.J., 1996. *Finite Element Procedures*. Prentice Hall, New Jersey.
- Belytschko, T., Liu, W.K. and Moran, B., 2001. *Nonlinear Finite Elements for Continua and Structures*. Wiley, New York.
- Borges, L.A., 1991. *Formulation and Solution for Limit Analysis considering Non Linear Yielding Surface (in portuguese)*. Ph.D. thesis, Pontificia Universidade Católica do Rio de Janeiro, Rio de Janeiro.
- Borges, L.A., Zouain, N., Costa, C. and Feijóo, R., 2001. "An adaptive approach to limit analysis". *ijss*, Vol. 38, No. 10-13, pp. 1707–1720. ISSN 0020-7683. URL <http://www.sciencedirect.com/science/article/B6VJS-423JJB2-6/2/4b13df41121aa8eb842cc5db151b2c36>. DOI: 10.1016/S0020-7683(00)00131-1.
- Borges, L.A., Zouain, N. and Huespe, A.E., 1996. "A nonlinear optimization procedure for limit analysis". *ejma*, Vol. 15, No. 3, pp. 487–512.
- Christiansen, E., 1996. "Limit analysis of collapse states". In P.G. Ciarlet and J.L. Lions, eds., *Handbook of Numerical Analysis. Vol. IV - Finite Element Methods (Part 2) - Numerical Methods for Solids (Part 2)*, Elsevier Science B.V., pp. 193–312.
- Han, W. and Reddy, B.D., 1999. *Plasticity: Mathematical Theory and Numerical Analysis*, Vol. 9 of *Interdisciplinary Applied Mathematics*. Springer.
- Hughes, T.J.R., 1987. *The Finite Element Method*. Prentice-Hall, Englewood Cliffs, N. J.
- Lembo, M. and Podio-Guidugli, P., 2001. "Internal constraints, reactive stresses, and the timoshenko beam theory". *Journal of Elasticity*, Vol. 65, pp. 131–148. ISSN 0374-3535. URL <http://dx.doi.org/10.1023/A:1016109822140>. DOI: 10.1023/A:1016109822140.
- Lubliner, J., 1990. *Plasticity Theory*. Macmillan, New York.
- Maier, G., Pastor, J., Ponter, A. and Weichert, D., 2003. "Direct methods of limit and shakedown analysis". In I. Milne, R.O. Ritchie, and B. Karahaloo, eds., *Comprehensive Structural Integrity*, Pergamon, Oxford, pp. 637 – 684. ISBN 978-0-08-043749-1. doi:DOI: 10.1016/B0-08-043749-4/03059-7.
- Sosa, J.L.C. and Gil, A.J., 2009. "Analysis of a continuum-based beam element in the framework of explicit-fem". *Finite Elements in Analysis and Design*, Vol. 45, No. 8-9, pp. 583–591.
- Zouain, N., 2004. "Shakedown and safety assessment". In E. Stein, R. de Borst and T.J.R. Hughes, eds., *Encyclopedia of Computational Mechanics*, John Wiley, chapter 9, pp. 291–334. ISBN 0-470-84699-2.

8. Responsibility notice

The author(s) is (are) the only responsible for the printed material included in this paper